Materials Research Express

PAPER

Continuous-flow precipitation as a route to prepare highly controlled nanohydroxyapatite: *in vitro* mineralization and biological evaluation

RECEIVED
6 October 2015

REVISED
7 April 2016

ACCEPTED FOR PUBLICATION
12 May 2016

PUBLISHED
21 July 2016

Filipa Castro[1,2,6], **Viviana P Ribeiro**[3,4,6], **António Ferreira**[1], **Ana L Oliveira**[3,4,5], **Rui L Reis**[3,4], **José A Teixeira**[5] **and Fernando Rocha**[1]

[1] LEPABE—Laboratory for Process Engineering, Environment, Biotechnology and Energy, Faculty of Engineering of the University of Porto, Rua Roberto Frias, s/n, 4200-465 Porto, Portugal
[2] CEB—Centre for Biological Engineering, University of Minho, Campus de Gualtar, 4710-057 Braga, Portugal
[3] 3B's Research Group—Biomaterials, Biodegradables and Biomimetics, University of Minho, Headquarters of the European Institute of Excellence on Tissue Engineering and Regenerative Medicine, AvePark 4806-909, Caldas das Taipas, Portugal
[4] ICVS/3B's—PT Government Associated Laboratory, Braga, Guimarães, Portugal
[5] CBQF—Center for Biotechnology and Fine Chemistry, School of Biotechnology, Portuguese Catholic University, Porto, 4200-401, Portugal
[6] Contributed equally to this study.

E-mail: filipaj@fe.up.pt **and** viviana.ribeiro@dep.uminho.pt

Keywords: nanohydroxyapatite, calcium phosphates, oscillatory flow reactor, mineralization, SBF

Abstract

This work reports the biological evaluation of nanosized hydroxyapatite (HAp) previously synthesized by continuous-flow precipitation in a scaled-up meso oscillatory flow reactor (meso-OFR). Physico-chemical characterization of the synthesized HAp suggests high surface reactivity namely because of its high specific surface area and low crystallinity. On the other hand, *in vitro* biomineralization assays demonstrated the apatite-forming activity of the prepared HAp and their higher surface reactivity when compared to a commercial HAp. Furthermore, human osteoblastic-like (Saos-2) cells culture evidenced that the synthesized HAp stimulated cell proliferation, especially when applied at lower concentrations (30 and 50 μg ml^{-1}), although its cellular uptake behavior. Therefore, the prepared HAp shows immense potential as biomedical material, as well as drug and gene delivery vehicle. The results are also very promising regarding further scaling up of the process, as the designed methodology allow for the preparation in a continuous mode of nanosized HAp with controlled physico-chemical properties.

Introduction

Calcium phosphates (CaPs) have been extensively used in biomedical applications, namely as substitute materials in dentistry and orthopaedic surgery for the regeneration of damaged hard tissues [1–3]. Hydroxyapatite (HAp), $Ca_{10}(PO_4)_6(OH)_2$, is the most well-known CaP since it shares similar chemical and crystallographic properties with the main inorganic component of bone and teeth enamel [2, 4, 5]. These attributes infer exceptional biocompatibility, bioactivity, and osteoconductivity [6], providing HAp the capability to lead to bone formation/mineralization and form bonds with the surrounding bone and connective tissues [7]. In this context, nanosized HAp has stimulated great interest in bone tissue engineering. Indeed, features of HAp nanoparticles are closer to features of biological HAp, since the mineral part of human bone is mainly made of nanostructured HAp crystals [2, 4, 8–12]. According to the literature, nanosized HAp has demonstrated to exhibit better biological properties when compared to that of coarser grained HAp [4, 9–12], promoting more readily osteointegration and subsequent bone tissue formation. Studies have reported that HAp nanoparticles exhibit improved sinterability and enhanced densification due to greater surface area [9, 10]. Further, nanosized HAp is expected to have better bioactivity when compared to microsized HAp [11, 12].

However, several other applications of HAp nanoparticles are also in progress. For instance, nanosized HAp demonstrates great potential as delivery vehicle for molecules such as proteins, drugs and DNA [11, 13]. Besides its established biocompatibility [13, 14], its high specific surface area and high surface reactivity promote an easy binding of great amount of molecules through simple adsorption [15–17]. In addition, its small size precludes immune system activation [13]. Due to its low solubility in physiological conditions, HAp provides a protective environment that shields molecules from degradation, while providing a pathway for controlled release [13, 16, 18]. More recently, surface modification of HAp nanoparticles has been performed through their conjugation with functional groups to provide a cell- or tissue- specific drug delivery [13]. In this way, concentration of drugs in the bloodstream is minimized and therefore systemic toxicity is reduced [16]. HAp nanoparticles composites have been prepared as well, to enhance and attribute additional properties, such as antimicrobial properties through silver incorporation [19, 20] and enhance osteoblasts function (like proliferation) by doping with metal ions [18]. Other functional properties such as photoluminescence [14, 15] and magnetism [21, 22] can be attributed to HAp nanoparticles through doping and magnetite material combining, enabling hence their use in bioimaging and cancer therapy, respectively.

Nanosized HAp particles can be prepared by a variety of methodologies including wet chemical precipitation, hydrothermal technique, sol-gel approach, microemulsion and solid-state reaction [12, 23, 24]. Among these methods, wet chemical precipitation is the most simplest route for the synthesis of nanozised HAp [24, 25]. Besides its low cost and easy application in industrial production [25], wet chemical precipitation has the advantage of a precise control over the morphology and size of particles [12]. However, precipitation from solution has the disadvantage of lacking control of the phase purity of nanoparticles [12, 26]. On the other hand, traditional wet mechanochemical processes usually lead to post-processing aggregation problems. Therefore, finding conditions for a controllable synthesis of nanosized HAp with specific characteristics is a relevant scientific and technological challenge [27].

Recently, we reported the preparation of HAp nanoparticles by continuous-flow precipitation in a scaled-up meso oscillatory flow reactor (OFR), under near-physiological conditions of pH and temperature [28]. The synthesized HAp nanoparticles show improved characteristics when compared to the HAp nanoparticles produced in a stirred tank batch reactor and a commercial HAp, namely a narrow size distribution and a mean size (d_{50}) of about 77 nm. The scaled-up meso-OFR used is based on a mesoscale (millilitre) device that was redesigned to suit some of the bioprocess applications requirements. The sharp baffles were replaced by smooth periodic constrictions (SPC), thus reducing the high shear regions that may be crucial to some cell cultures. The straight tube and the smooth periodic constrictions were incorporated as a single piece, thus making it easy for sterilisation. Additionally, the meso-OFR has been proved to result into significant enhancement in processes such as mass transfer and particle mixing [29–31] due to its efficient mixing mechanism (oscillatory flow mixing). The liquid or multiphase fluid is typically oscillated in the axial direction and this motion interacts with the constrictions forming vortices, mixing intensity being controlled by the oscillation frequency and amplitude. In turn, traditional stirred tank batch reactors usually employed for the production of synthetic HAp often lead to inconsistences in product specifications due to their low mixing efficiency [32]. Furthermore, batch mode operation provides only limited amounts of material and crystallization conditions may change during multiple syntheses, while continuous mode operation allows a more efficient use of reagents and enhanced reproducibility of results because all material crystallizes under uniform conditions [33].

In the present work, the biological evaluation of the HAp nanoparticles prepared in the scaled-up meso-OFR is assessed as an alternative route for commercially solutions presently available in the market for biomedical purposes. A comparative study was developed to evaluate the effect of the HAp particles on cell viability, proliferation and morphology (MTS, DNA and SEM analysis). In addition, simulated body fluid (SBF) studies up to 60 days were carried out in order to provide an indication of the *in vitro* mineralization potential of the synthesized HAp nanoparticles.

Experimental section

HAp nanoparticles synthesis

HAp nanoparticles were synthesized by continuous-flow precipitation in a scaled-up meso-OFR with an approximate volume of 30 ml (figure 1). The nanoparticles were obtained by mixing a saturated calcium hydroxide (Sigma-Aldrich, 95%) aqueous solution (0.019 26 M) and an orthophosphoric acid (Sigma-Aldrich, 85%) aqueous solution (0.011 54 M). The initial mixing molar ratio Ca/P was 1.33 and the residence time τ was 3.3 min. The mixing conditions, i.e., the frequency, f, and the amplitude, x_0, were fixed at 1.83 Hz and 4.5 mm, respectively. Experiments were conducted under near-physiological conditions of temperature (37 °C) and pH (6.65), which is particularly relevant when preparing HAp for medical purposes. It is important to underline that the HAp nanoparticles were used as-prepared, without thermal treatment and without granulometric

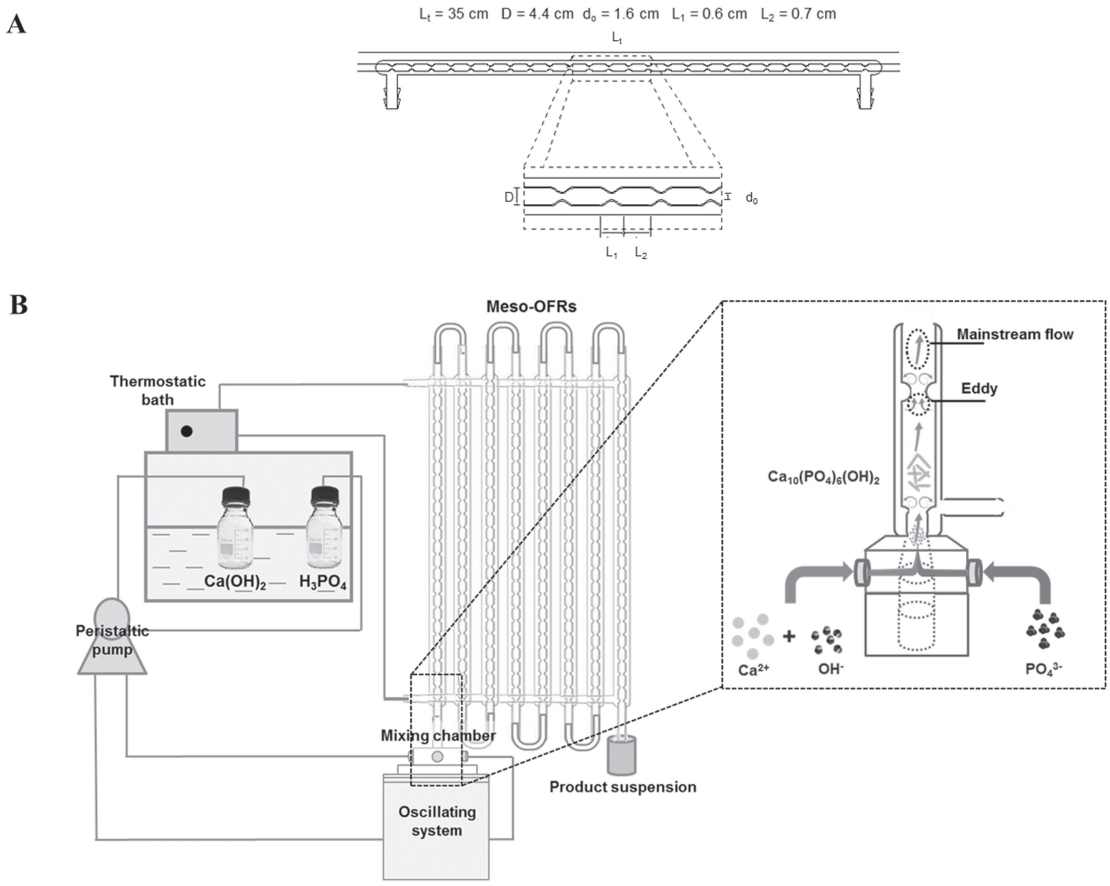

Figure 1. (A) Schematic representation of the meso oscillatory flow reactor (meso-OFR) and (B) experimental installation for the continuous-flow precipitation of HAp (based on Castro *et al* [28]).

separation. Further details on the experimental installation as well as the methodology can be found in Castro *et al* [28].

HAp nanoparticles characterization

Suspensions were withdrawn at the outlet of the meso reactor, centrifuged (at 1500 rpm for 5 min), and washed twice with ultrapure water and pure ethanol (99.8%), which stops the solid−liquid reaction[21]. The precipitate was then dried overnight at 60 °C and weighed for the estimation of the mass of the crystals obtained, giving an approximate yield of 1 mg ml^{-1}. The obtained powder and a commercial HAp (Calcium hydroxyapatite, Spectrum, minimum 40 meshes, $Ca_5HO_{13}P_3$) were characterized by x-ray diffraction (XRD; PanAlytical X'Pert PRO Alfa-1 diffractometer with λ Cu Kα = 1.540 56 Å), Fourier transform infrared spectroscopy (FTIR; Bomem MB-154S), and scanning electron microscopy (SEM; FEI Quanta 400FEG ESEM/EDAX Genesis X4M with an accelerating voltage of 15 kV and 20 kV), where samples were covered by a 10 nm layer of gold. The Ca/P molar ratio was calculated for both synthesized and commercial HAp, after dissolving the powders in 0.5 M HCl solution and quantifying the amount of calcium (Ca) and phosphorus (P) present. Atomic absorption spectroscopy (AA400, Perkin-Elmer, Norwalk, CT) was used to quantify the amount of Ca at 422.7 nm. To eliminate the interference of phosphate in the measurement of calcium, 0.1 ml of the sample solution was diluted in 5 ml of 0.625% wt of $LaCl_3$ that acts as a release agent. The P concentration was analyzed by the 'molybdenum blue' method [34] using a UV-light spectrophotometer (Shimadzu UV 1800), at 820 nm. For both methods, 3 replicates were analyzed and the average values calculated. Multi point Brunauer–Emmett–Teller (BET) surface area measurements were also performed on a Quantachrome Autosorb AS-1 instrument at −196 °C. Prior to the analysis the samples were outgassed in vacuum at 300 °C for 2 h. Regarding particle size distribution, both synthesized and commercial HAp were analysed by laser diffraction (LS 230, Beckman Coulter).

Table 1. Nominal ion concentrations of SBF in comparison with those in human blood plasma.

	Ion concentrations (mM)	
Ion	Blood plasma	Simulated fluid
Na^+	142.0	142.0
K^+	5.0	5.0
Mg^{2+}	1.5	1.5
Ca^{2+}	2.5	2.5
Cl^-	103.0	147.8
HCO^{3-}	27.0	4.2
$HPO_4{}^{3-}$	1.0	1.0
$SO_4{}^{2-}$	0.5	0.5

In vitro mineralization

According to Kokubo and Takadama [35], the potential *in vivo* bioactivity of a biomaterial may be inferred by its ability to form apatite on its surface whilst immersed in simulated body fluid (SBF). Although SBF does not simulate accurately the physiological conditions [36] and some materials have shown not to mineralize in the presence of SBF [37, 38], the presence of *in vitro* mineralization is considered a strong indication of *in vivo* mineralization ability. In this way, a SBF solution was prepared in laboratory according to the Kokubo method [35]. Table 1 gives the ion concentration of SBF and its comparison with human blood plasma. Also, its pH was adjusted to 7.40 exactly at 36.5 °C. *In vitro* assays were then achieved by soaking 100 mg of HAp powder into 100 ml of SBF solution maintained at 37 °C and under agitation at 50 rpm. HAp particles were incubated for various time periods (0, 1, 3, 7, 15, 30 and 60 days), without refreshing or adding SBF solution. After incubation for a particular time period, the samples were centrifuged at 5000 rpm for 5 min, and after decanting the supernatant, the particles were washed with ultra-pure water, and then with ethanol to stop the reaction. The drying was achieved in an oven at 60 °C during 24 h. Assays were carried out in triplicate for both synthesized and commercial HAp particles (Calcium hydroxyapatite, Spectrum, minimum 40 meshes, $Ca_5HO_{13}P_3$), assessed as a control condition. The SBF solution collected at each time point was characterized by Inductively Coupled Plasma Optical Emission Spectroscopy (ICP-OES—Horiba Jobin Yvon Activa M) to evaluate the ionic exchange between HAp particles and SBF liquid, and the physico-chemical properties of the powders were studied by Fourier transform infrared spectroscopy (FTIR—Bomem MB-154S), x-ray diffraction (XRD—PanAlytical X'Pert PRO Alfa-1 diffractometer with λ Cu K$\alpha = 1.540\,56$ Å) and Scanning Electron Microscopy (SEM—FEI Quanta 400FEG ESEM/EDAX Genesis X4 M with an accelerating voltage of 20 kV).

In vitro cytotoxicity and cell behavior

- Seeding and exposure of Saos-2 cells to HAp nanoparticles
  A human osteoblastic osteosarcoma cell line (Saos-2), was used to assess the eventual cytotoxicity and cell behavior in the presence of the produced HAp nanoparticles. For that purpose, cells were grown as monolayer cultures in standard basal medium consisting of Dulbecco's Modified Eagle's Medium (DMEM; Sigma Aldrich, Germany) supplemented with 10% fetal bovine serum (FBS; Biochrom AG, Germany) and 1% antibiotic-antimycotic solution (Gibco, GB). At confluence, cells were detached from the culture flasks using TrypLE Express enzyme with phenol red (Life Technologies, Carlsbad, CA), centrifuged, ressuspended in culture medium and seeded in 48-well cell culture plates (Falcon) at a density of 1×10^4 cells cm^{-2}. After 24 h of attachment, cells were cultured under static conditions in basal medium supplemented with different concentrations (30 μg ml^{-1}; 50 μg ml^{-1}; 100 μg ml^{-1} and 200 μg ml^{-1}) of HAp particles, prepared in the meso-OFR and commercial HAp (Calcium hydroxyapatite, Spectrum, minimum 40 meshes, $Ca_5HO_{13}P_3$), assessed as control condition. Cells were cultured for 1, 3 and 7 days in the presence of the tested HAp particles. Tissue culture polystyrene (TCPS; Sarstedt, USA) coverslips were used to assess cell morphology by SEM.
- MTS assay
  A 3-(4,5-dimethylthiazol-2-yl)-5-(3-carboxymethoxyphenyl)-2-(4-sulfophynyl)-2H-tetrazolium) (MTS) assay was performed to evaluate the cytotoxicity of the synthesized and commercial HAp particles in comparison to latex (positive control for cell death). After 1, 3 and 7 days of culture, the culture medium was removed and replaced by 300 μl of mixed solution containing serum-free culture medium (without phenol red) and MTS (CellTiter 96 One Solution Cell Proliferation Assay Kit, Promega, PA, USA). After incubation for 3 h at 37 °C in an atmosphere with 5% CO_2, the optical density (OD) was measured at 490 nm using a plate

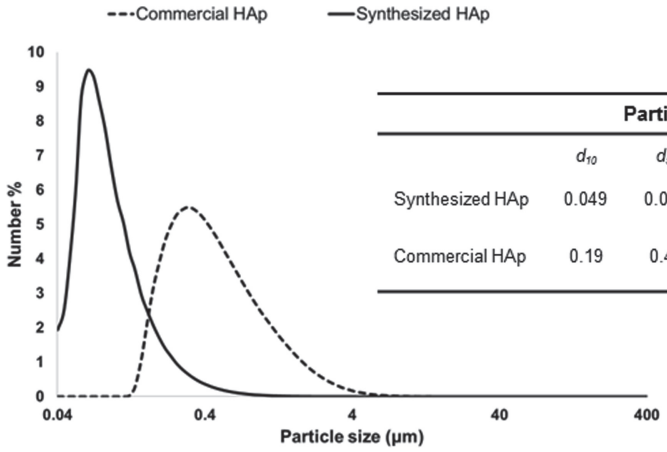

	Particle size (µm)			
	d_{10}	d_{50}	d_{90}	Span
Synthesized HAp	0.049	0.077	0.172	1.60
Commercial HAp	0.19	0.40	1.22	3.03

Figure 2. Particle size distribution in number of both synthesized and commercial HAp.

reader (Molecular Devices, CA, USA). Cell viability was calculated by subtracting the mean OD value of the blank (samples without cells) from the ones of the tested concentrations of synthesized HAp and controls. The MTS assay was performed in triplicate.

- DNA assay
  Saos-2 cell proliferation was assessed by using a fluorimetric double-strand DNA quantification kit (PicoGreen, Molecular Probes, Invitrogen Corporation, USA) following manufacturer's instructions. Samples previously frozen at −80 °C were thawed at room temperature and the supernatant fluorescence measured (485 nm excitation and 528 nm emission) in a microplate reader (Synergy HT, BioTek Instruments, USA). DNA amount was calculated according to a standard curve and by subtracting the fluorescence measurements of samples without cells. The DNA assay was performed in triplicate.
- Cell morphology and distribution by SEM

After each pre-defined culturing time, the cell-seeded TCPSs were washed with Phosphate Buffered Saline (PBS; Sigma, USA) and fixed with 2.5% glutaraldehyde (Sigma, USA) solution in PBS. After rising again with PBS, samples were dehydrated using a series of ethanol solutions (30%, 50%, 60%, 70%, 80%, 90% and 100% v/v) and treated with hexamethylidisilazane (HMDS; Electron Microscopy Sciences, USA). Samples were sputter coated with gold (Fisons Instruments, Sputter Coater SC502, UK) prior to analysis using a Leica Cambridge S360 Scanning Electron Microscope and the micrographs were taken at an accelerating voltage of 15 kV at different magnifications.

Results and discussion

Physico-chemical properties of synthesized HAp

Synthetized HAp nanoparticles were previously characterised [28] in terms of their size (figure 2) and morphology (figures 3(C) and (D)). Results show that the synthesized HAp has a lower mean size (d_{50} of about 77 nm) than the commercial HAp (d_{50} of about 400 nm). They also evidence that the synthesized HAp is constituted by aggregated rod-like shaped nanoparticles (of about 100 nm long and 20 nm width), while the commercial HAp is characterized by aggregated rod-like shaped microsized particles.

Table 2 presents the estimated Ca/P molar ratio as well as the specific surface area (SSA) of both synthesized and commercial HAp. Results evidence that both HAp powders have a Ca/P molar ratio higher than the stoichiometric value (1, 67), suggesting thus carbonate substituted hydroxyapatite, characteristic similar to the apatite phase present in natural bone [11, 27, 39]. Additionally, it is possible to verify that the synthesized HAp has a lower amount of calcium when compared to the commercial HAp. Results also indicate that the prepared HAp has a higher specific surface area than the commercial HAp.

Concerning phase identification and crystallinity, FTIR spectra (figure 4) and XRD patterns (figure 5) of both synthesized and commercial HAp (referred as synthesized HAp 0 days and commercial HAp 0 days) suggest that both powders are constituted by low crystalline calcium-deficient carbonated hydroxyapatite. From figure 4 FTIR spectra exhibit apatite characteristic absorption bands [40], namely bands assigned to the phosphate group PO_4^{3-} at 962–1100 cm^{-1} and the hydroxyl group OH^- at 3571 and 630 cm^{-1}. Broadening of the PO_4^{3-} bands

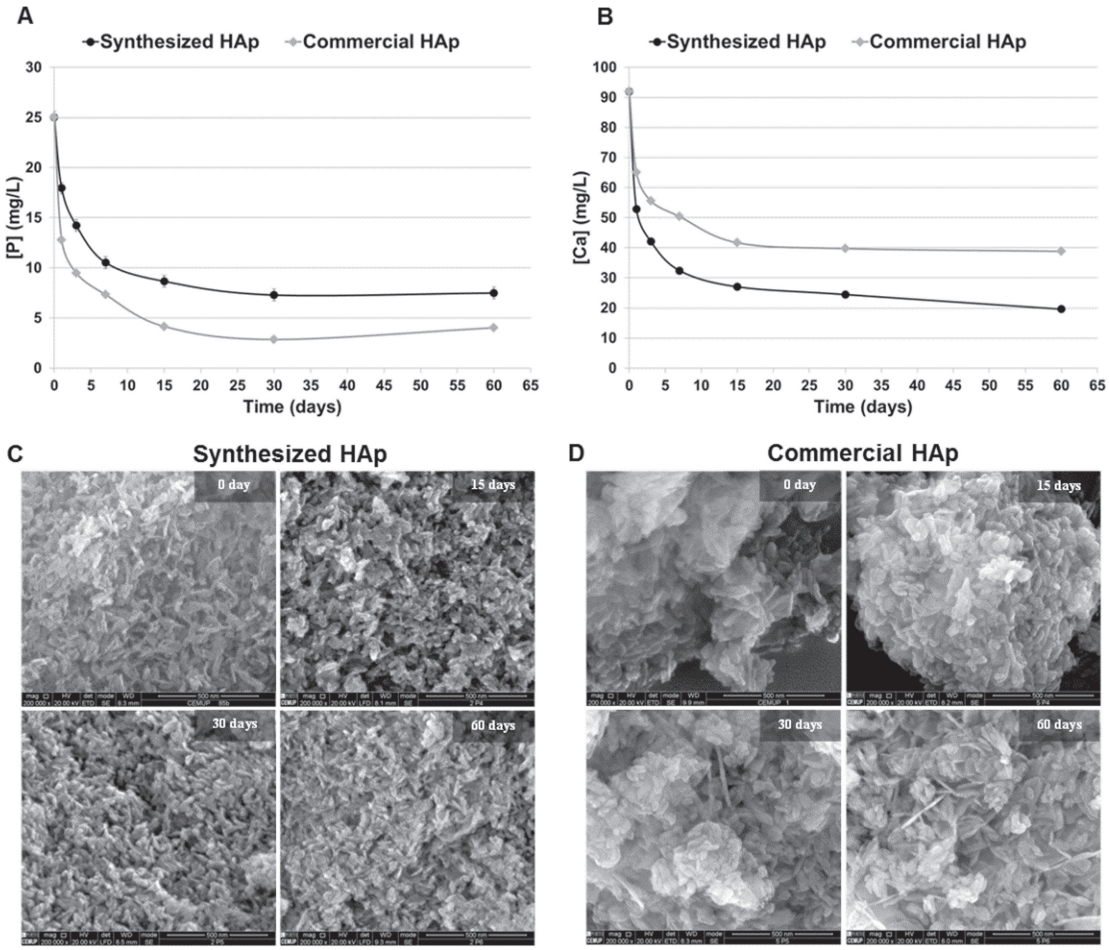

Figure 3. Variation of elemental concentration of phosphorus (P) (A) and calcium (Ca) (B) in SBF as function of soaking time (the error bars are standard deviations from three independent experiments). SEM images of both (C) synthesized and (D) commercial HAp, at different times of immersion in SBF.

Table 2. Ca/P molar ratio and specific surface area (SSA) of both synthesized and commercial HAp.

	Ca/P molar ratio	SSA ($m^2\ g^{-1}$)
Synthesized HAp	1.72	70, 8
Commercial HAp	1.87	53, 3

indicates small size and low crystallinity of both HAp powders [41, 42]. The peak assigned to the stretching mode υ_S (3571 cm^{-1}) of OH^- is not evidenced in the spectrum of the synthesized HAp, which may be due to an overlap with the broad peak of the adsorbed water around 3700–3000 cm^{-1}. Presence of adsorbed water is also confirmed by the existence of a peak at 1643 cm^{-1}, assigned to the bending mode υ_2 of HOH. In the case of the prepared HAp, this could be related to the process itself, as experiments were performed at low temperature and without a ripening (ageing) treatment [28]. Absorption bands were also observed at 1455 and 1420 cm^{-1}, especially in the spectra of the commercial HAp. Those are due to the stretching and bending modes of C–O and P–O bonds and air carbonated CO_3^{2-} ions. In addition, the peak around 875 cm^{-1} can be assigned to the vibrational frequencies of carbonate (CO_3^{2-}) or hydrogen phosphate (HPO_4^{2-}) ions. As to the peak observed around 2360 cm^{-1}, it is associated to the atmospheric CO_2. Figure 5 shows the XRD patterns of both synthesized and commercial HAp powders. The diffraction peaks were identified using a reference pattern for HAp (JCPDS 9-0432). All the major peaks of HAp are present in both XRD patterns along with a few minor peaks corresponding to carbonated HAp. One can also remark that diffraction peaks are markedly broader in the case of the synthesized HAp, which may indicate smaller size and lower crystallinity when compared to the commercial HAp. Besides, peaks assigned to KCl (namely at 28° 2θ and 40.5° 2θ) were observed in the diffraction pattern of the produced HAp. As mentioned in a previous work [28], this may be due to the occlusion

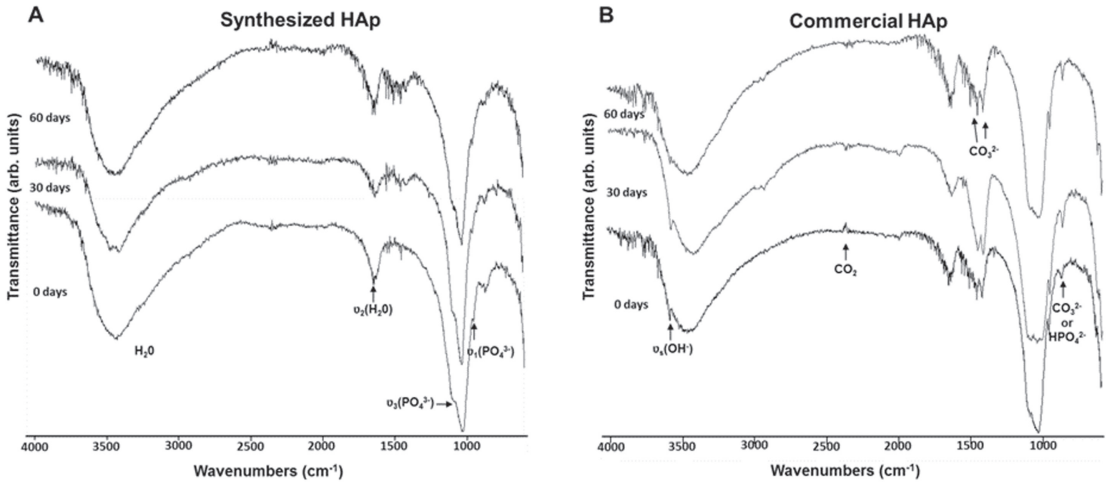

Figure 4. FTIR spectra of both synthesized (A) and commercial (B) HAp, at different times of immersion in SBF.

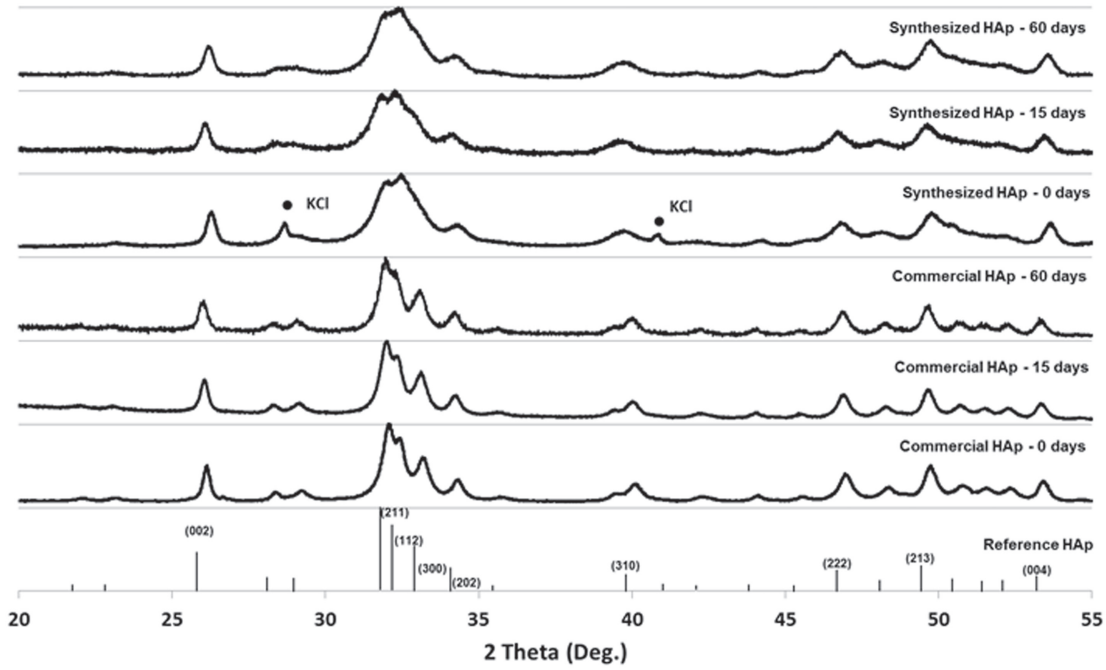

Figure 5. XRD patterns of both synthesized and commercial HAp, at different times of immersion in SBF.

of KCl present in the mother liquor, which could have been trapped in the aggregated particles and crystallized at the drying step.

In vitro mineralization

Figure 3 shows the variation in calcium (Ca) and phosphorus (P) ion concentrations in the SBF solution as function of the immersion time for both synthesized and commercial HAp particles. A significant decline in both Ca and P ion concentrations was observed from the first day of immersion. After 30 days of immersion the Ca and P ion levels in the SBF solution became approximately constant for both powders studied. Further, the overall depletion rate of Ca ion concentration from the SBF solution was higher for the prepared HAp than the commercial HAp (figure 3(B)), while the decrease in P ion concentration from the SBF was more pronounced for the commercial HAp (figure 3(A)). The decrease in Ca and P concentrations in SBF solution may indicate that these ions were accumulated on the surface of the HAp particles. This accumulation due to the electrostatic attraction increases the supersaturation near the HAp surface, leading, as a result, to the precipitation of a new CaP phase [43]. As observed in these experiments, precipitation seems to start almost immediately after

immersion, although the assessment of Ca and P ion concentration was only done after 1 day of immersion. According to Kim [44], precipitates can immediately form when the HAp powders are soaked in SBF. In fact, the isoelectric point of HAp in water is at pH ranging between 5 and 7 [45], lower than the pH of the SBF (7.4). Therefore, once immersed in SBF HAp exhibits negative surface charge by exposing hydroxyl and phosphate groups [45]. This negative charge interacts with the positive Ca ions in the fluid, making the surface acquire positive charge, which in turn interacts with the negative phosphate ions. Regarding the consumption rate of Ca ions, this might be affected by the magnitude of the initial surface negativity of HAp [44]. As described above, the prepared HAp has a lower calcium content, suggesting thereby a more negative surface when compared to the commercial HAp [46, 47]. Moreover, the lower dimensions (figures 2 and 3) and the higher surface area (table 2) of the synthesized HAp particles make them to adsorb more ions on their surface, leading to an increased degree of supersaturation of the surrounding fluid with respect to apatite, and thus accelerating the precipitation process [27, 39, 48]. The surface reactivity of the synthesized HAp may also be attributed to the existence of adsorbed water on its surface [28], constituting an ion reservoir for the growth of a new apatite phase [49]. Concerning the phosphorus consumption rate, it follows the same trend as the calcium consumption rate for both powders. This can be explained by the consumption of both calcium and phosphorus upon the deposition of a CaP layer at the surface of both synthesized and commercial HAp particles.

Figures 3(C) and 2(D) represent SEM images of both synthesized and commercial HAp particles immersed in SBF for 0, 15, 30 and 60 days. Figure 3(C) shows a regular distribution of aggregated rod-like nanoparticles before and after soaking in SBF for the produced HAp. Regarding the commercial HAp (figure 3(D)), it is mainly formed by highly aggregated rod-like microparticles, unless after 30 and 60 days of immersion in SBF where the presence of microsized plate-like particles is verified. This may indicate the formation of a new CaP phase or phase transformation, although HAp can exhibit various sizes and shapes [12]. Regarding aggregation of the particles, it is probably attributed to their high surface-area-to-volume ratio, which results in a high surface tension that they tend to lower by adhering to one another [50]. Furthermore, SEM images evidence that the synthesized HAp particles are smaller and uniformly distributed in size when compared with the commercial HAp. This was also confirmed by HAp particles size distribution data for both HAps without soaking in SBF (figure 2), where the synthesized HAp exhibits a lower mean size and a narrower size distribution than the commercial HAp. Indeed, the efficient oscillatory mixing mechanism developed in the meso-OFR leads to a more homogeneous reaction medium and therefore to a more homogeneous distribution of supersaturation, promoting thus monodispersity of the synthesized nanoparticles [51].

FTIR spectra of both synthesized and commercial HAp at different times of immersion in SBF are illustrated in figure 4. Results suggest that the powder obtained after immersion in SBF is calcium-deficient carbonated HAp, regardless of the immersion time. Beyond apatite characteristic absorption bands (already described in detail above) [40], all the spectra exhibit carbonate (CO_3^{2-}), particularly the commercial HAp spectra, and/or hydrogen phosphate (HPO_4^{2-}) ions bands. Once formed in SBF, the new CaP phase grows spontaneously consuming the calcium and phosphate ions and may incorporate minor ions such as carbonate from ambient carbon dioxide solubilization [8]. In addition, broadening of the bands, especially phosphate bands (more pronounced in the commercial HAp spectra) and presence of water peaks indicate low crystallinity.

Figure 5 shows the XRD patterns of both synthesized and commercial HAp powders after 0, 15 and 60 days of soaking in SBF solution at 37 °C. Results obtained show the formation of low crystalline carbonated HAp for both powders immersed in SBF, once all the patterns exhibit all the major peaks of apatite phase and few minor peaks corresponding to carbonated HAp. One can also verify that peak broadening is more marked in the synthesized HAp, suggesting low crystallinity and small crystal size.

The results obtained suggest thus that both synthesized and commercial HAp powders support the precipitation of small size and low crystalline carbonated and/or calcium-deficient HAp on their surface, characteristics similar to the apatite phase present in natural bone [11, 27, 39]. It is important to underline that unlike the commercial HAp, the synthesized HAp was collected as-prepared without further treatment such as ripening (ageing) process and dried at a low temperature.

In vitro cytotoxicity and cell behavior

Saos-2 cells, a widely used permanent line of human osteoblastic-like cells [52], were cultured in direct contact with different concentrations of both synthesized and commercial HAp particles for 1, 3 and 7 days. The eventual cytotoxic events and biological behavior were assessed through MTS and DNA quantification and SEM qualitative analysis. MTS analysis showed that no cytotoxic events were registered (figure 6(A)). In fact, a significant increase in cell activity was observed over the culture period for all tested conditions ($p < 0.05$, $p < 0.01$, $p < 0.001$). In this study, no significant differences were obtained between the developed HAp nanoparticles and the commercial HAp, except at the concentrations of 30 and 50 μg ml^{-1}, where cell activity was significantly higher ($p < 0.05$) for cells cultured on the developed HAp nanoparticles. DNA quantification

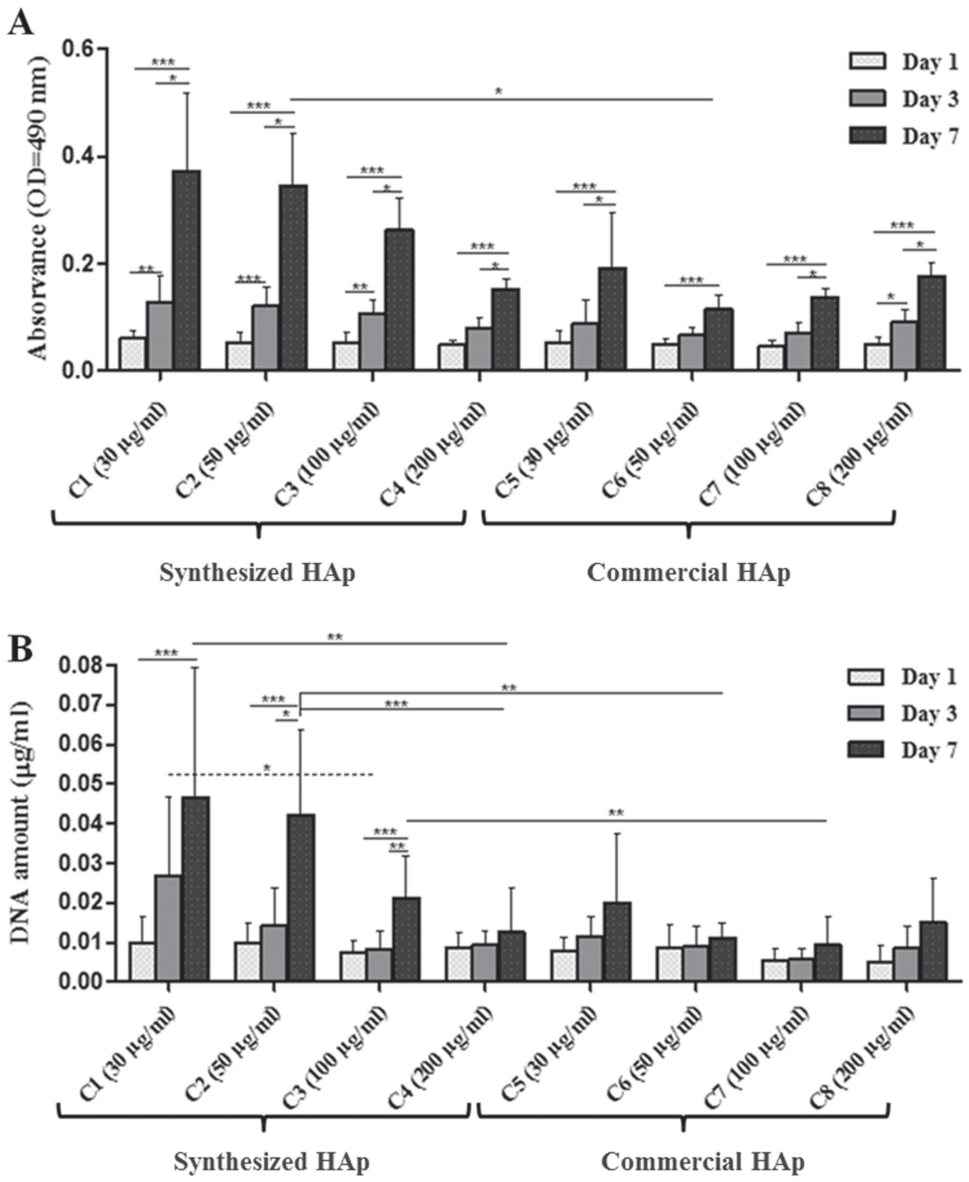

Figure 6. Cell viability and proliferation measured by (A) MTS test and (B) DNA quantification, respectively, for Saos-2 cells cultured in direct contact with synthesized and commercial HAp particles, for 1, 3 and 7 days of culture. Data were analysed as mean ± standard deviation with n = 9 for each bar. Statistical analysis was performed with GraphPad Prism 5.0 (GraphPad Software) using the Kruskal-Wallis test followed by Dunn's method as Multiple Comparision post-test. The significance level was $^{*}p < 0.05$, $^{**}p < 0.01$, $^{***}p < 0.001$.

results (figure 6(B)) showed that after 24 h of exposure at varying concentrations of synthesized and commercial HAp particles, no significant differences were observed between all the tested conditions. After 3 days of culture a notorious increase in cell proliferation was observed on C1 condition, at significant levels ($p < 0.05$) as compared to C3 condition. No significant differences were obtained between the remaining tested systems and the proliferation rate was not significantly different between day 1 and day 3 of culture. After 7 days of culture, the proliferation rate was significantly higher on C1 ($p < 0.01$) and C2 ($p < 0.001$) conditions, in comparison to the highest concentration of the prepared HAp nanoparticles (C4). Moreover, the DNA content was significantly higher ($p < 0.01$) for cells cultured on the synthesized HAp nanoparticles at the concentrations of 30 and 50 μg ml^{-1}, as compared to the commercial HAp. The DNA values were also significantly higher ($p < 0.05$, $p < 0.01$, $p < 0.001$) for the prepared HAp conditions (except for C4) on day 7, compared to the early culture periods. These results are consistent with those reported by Depan *et al* [41] where pre-osteoblastic cells cultured for 7 days in the presence of a HAp-chitosan (CS)–graphene oxide (GO) system showed an increase of metabolic activity, as compared to the pure non-biomineralized system. Chen *et al* [42] also observed that MC3T3-E1 cells viability increased over 7 days of culture in the presence of increasing concentrations (0–1 mg ml^{-1}) of uncharged HAp nanoparticles. The same cell behavior was observed for cells cultured on differently charged HAp nanoparticles with dosage of 1 mg ml^{-1}. In another study, Cai *et al* [4] observed an increase of bone

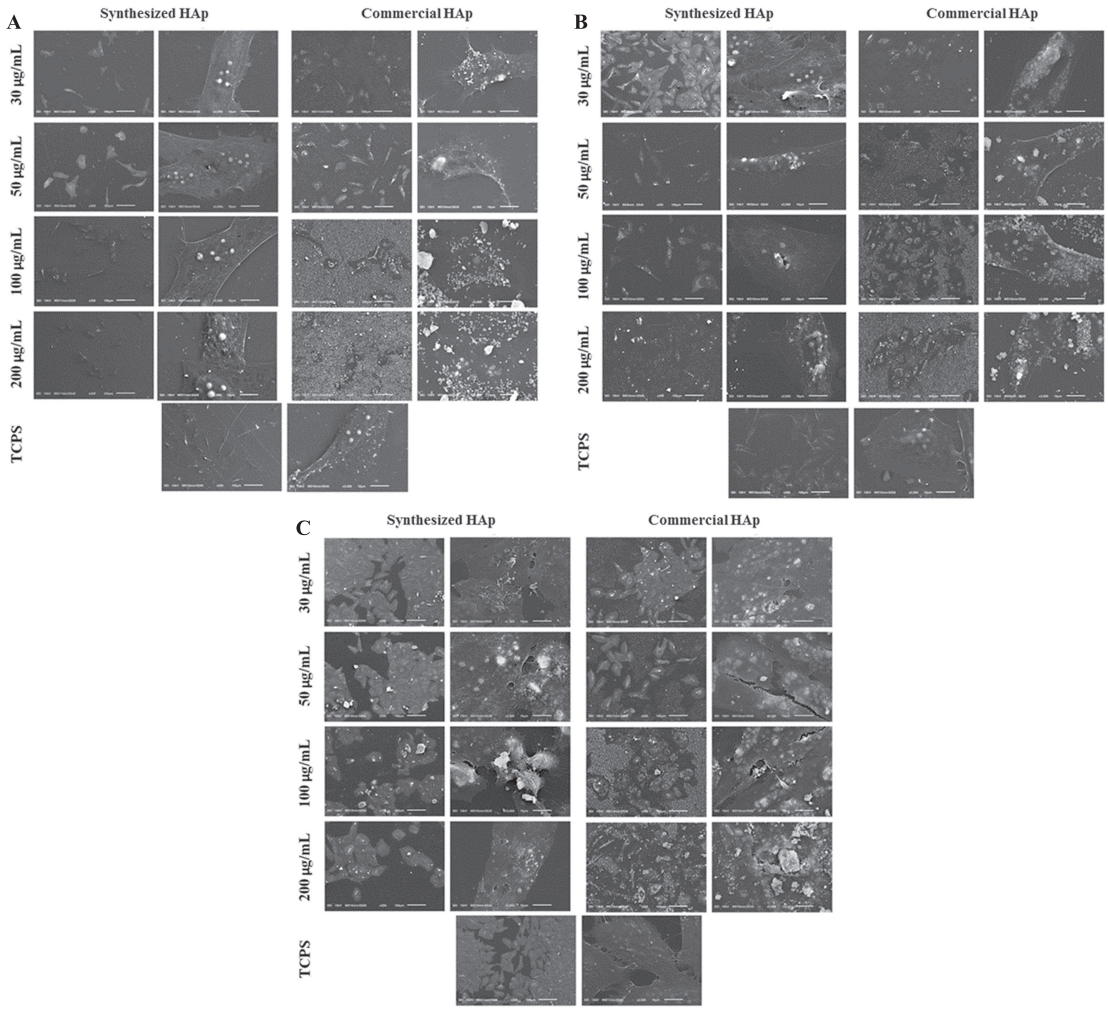

Figure 7. SEM micrographs illustrating the morphology, distribution and proliferation of Saos-2 cells cultured in direct contact with synthesized and commercial HAp particles, for (A) 1 day; (B) 3 days (C) and 7 days of culture.

marrow mesenchymal stem cells (MSCs) and osteosarcoma cells (U2OSs) proliferation after 7 days of culture on HAp nanoparticles with different average diameters. On the other side, Shi *et al* [53] verified that HAp particles size influences greatly the proliferation of human osteoblast-like MG-63 cells, nanosized HAp having the best effect on the proliferation rate when compared to microszied HAp. This is in agreement with the results obtained, as best proliferation rates were observed for cell cultured on the prepared HAp particles. Indeed, synthesized HAp was proven to be nanosized (see figures 2 and 3) and has a higher specific surface area (see table 2) when compared to the commercial HAp, which promotes cell attachment and thereby may explain the higher proliferation rate and activity observed. Therefore, it is suggested that the synthesized HAp nanoparticles can exhibit a favorable influence over cell proliferation rate and activity, in which the size and concentration rate are believed to play a key role.

The analysis of SEM results (figure 7) confirmed cell-material interactions over the culture period for all the tested concentrations, once cells were able to attach and spread on both types of HAp particles exhibiting a flat appearance. After 1 day of cell culture, the cell spreading can be viewed as exhibiting a flat appearance for all the tested conditions (figure 7(A)). After 3 days of culture, a notorious proliferation was observed on the synthesized HAp–30 μg ml^{-1} system (figure 7(B)), which is consistent with the results obtained by DNA quantification analysis. However no major differences were observed between the remaining tested conditions. HAp particles have gained a particular reputation as bone substitute materials. Depending on the particle size, the HAp may play a different role in the regeneration of bone-defect areas. It has been reported that HAp particles can facilitate bone remodeling induced by osteoclasts and osteoblasts [54]. Balasundaram and colleagues [55] also studied nanosized and low crystalline calcium phosphate based materials. They reported that small size and low crystalline HAp may promote osteoblast adhesion to the same degree as the well-established techniques of functionalizing conventional HAp with RGD. Beyond the already mentioned advantages of nanosized HAp in promoting a higher surface area for cell adherence, surface chemistry and topography of lower crystallinity is

favorable for cell attachment [56]. Namely, the existence of a hydrated surface layer on the produced HAp increases the number of adsorption sites [49]. Concerning cell morphology, Depan *et al* [41] observed that after 1 day of pre-osteoblasts seeding in the presence of a HAp-CS–GO system, the cell spreading can be viewed as exhibiting a predominantly flat appearance with significant cytoplasm, which was also verified in this work. In their turn, Shi *et al* [53] investigated the influence of HAp nanoparticles size in MG-63 cell line morphology after 5 days of culture. MG-63 cells presented a polygonal form with fine filopodia and abundant surface folds on particles with diameters of 20 nm, while spherical or round cells with fewer filopodia were observed on particles with diameters of 80 nm, presenting some morphological changes, such as swollen mitochondria, deformed nucleus and condensed chromatin. In addition, figure 7(C) clearly demonstrates that Saos-2-cultured for 1 week actively involved and phagocytized the HAp particles, while extending many projections. By contrast, Hatakeyama *et al* [3] reported that Saos-2 cells actively phagocytized nanosized HAp/Col composites only after 4 weeks of culture, appearing as spheroids with cytoplasmic projections. As shown in figure 7(C), cells preferentially covered and spread over the aggregated HAp particles after 1 week of culture. In a different study, Chen *et al* [42] revealed by transmission electron microscopy (TEM) analysis that MC3T3-E1 cell line was able to encapsulate different charged HAp nanoparticles after 3 days of culture with similar size and shape (100 nm in length, 20 nm in diameter) as the prepared HAp.

The results presented above are thereby very encouraging regarding biomedical applications, since besides *in vitro* apatite-forming activity, the synthesized HAp nanoparticles stimulated cell proliferation. Moreover, the designed processing conditions can allow for the precise control of the nanoparticles size, in a continuous mode production. This aspect is very important thus allowing for the scaling up and further industrialization of the system without compromising physico-chemical properties of the obtained HAp and eliminating batch to batch variability.

Conclusions

In the present work, HAp nanoparticles previously produced by a wet chemical precipitation in a scaled-up meso oscillatory flow reactor (meso-OFR) operating in continuous mode and a commercial HAp, assessed as a control condition, were tested to evaluate their biological activity and effects over cell viability and proliferation.

Physico-chemical characterization show that both synthesized and commercial HAp are calcium-deficient carbonated HAp, although calcium content of the synthesized HAp is lower. In addition, results confirm the smaller size and higher specific surface area of the synthesized HAp when compared to the commercial HAp. Furthermore, *in vitro* mineralization studies evidenced the formation of a bone-like apatite on the surface of both HAp powders, in the presence of SBF, revealing that both types of particles have *in vitro* apatite-forming activity. Different concentrations of both synthesized and commercial HAp particles were used to evaluate the *in vitro* biological behavior of human Saos-2 osteoblast-like cells. All the tested HAp powders induced a positive influence over cell activity and proliferation. Nevertheless, synthesized HAp nanoparticles applied at lower concentrations have the greatest potential over cell behavior, although their internalization by cells was observed. Furthermore, *in vitro* mineralization studies evidenced the higher surface reactivity of the synthesized HAp over the commercial.

The present work may provide improved understanding of the functional properties of nanobiomaterials and the potential applications of HAp nanoparticles from biomedical materials to delivery vehicles and bioimaging. The results are also very promising regarding the designed HAp preparation methodology, as HAp nanoparticles with controlled physico-chemical properties were synthesized in a continuous mode, allowing thus further scaling up of the system without compromising properties of the resulting HAp.

Acknowledgments

This work was financially supported by the European Regional Development Fund (FEDER) through COMPETE 2020—Operational Programme Competitiveness and Internationalization (POCI) (UID/EQU/00511/2013-LEPABE—Laboratory for Process Engineering, Environment, Biotechnology and Energy—EQU/00511; POCI-01-0145-FEDER-006684) and by national funds through FCT—Portuguese Foundation for Science and Technology—under the projects: UID/BIO/04469/2013 (FC); PEst-C/SAU/LA0026/2013 project (VPR); IF exploratory project IF/01087/2014; Postdoctoral Fellowship SFRH/BPD/96132/2013 (FC); Doctoral Scholarship PD/BD/113806/2015, FCT/MCTES and FSE/POCH, PD/59/2013 (VPR). A Ferreira and A L Oliveira are Investigators FCT (ALO: IF/00411/2013; AF: IF/01087/2014). The authors are thankful to Dr Jorge Ferreira from LNEG (Laboratório Nacional de Energia e Geologia, Portugal) for carrying out the x-ray measurements and his help with the interpretation of results, and to Cátia Azenha from LEPABE-FEUP for carrying out the Multi point Brunauer–Emmett–Teller (BET) surface area measurements.

References

[1] Castro F, Ferreira A, Rocha F, Vicente A and António Teixeira J 2012 Characterization of intermediate stages in the precipitation of hydroxyapatite at 37 °C *Chem. Eng. Sci.* **77** 150–6
[2] Cox S C, Jamshidi P, Grover L M and Mallick K K 2014 Preparation and characterisation of nanophase Sr, Mg, and Zn substituted hydroxyapatite by aqueous precipitation *Mater. Sci. Eng. C. Mater. Biol. Appl.* **35** 106–14
[3] Hatakeyama W, Taira M, Chosa N, Kihara H, Ishisaki A and Kondo H 2013 Effects of apatite particle size in two apatite/collagen composites on the osteogenic differentiation profile of osteoblastic cells *Int. J. Mol. Med.* **32** 1255–61
[4] Cai Y, Liu Y, Yan W, Hu Q, Tao J, Zhang M, Shi Z and Tang R 2007 Role of hydroxyapatite nanoparticle size in bone cell proliferation *J. Mater. Chem.* **17** 3780
[5] Zhao X, Ng S, Heng B C, Guo J, Ma L, Tan T T Y, Ng K W and Loo S C J 2013 Cytotoxicity of hydroxyapatite nanoparticles is shape and cell dependent *Arch. Toxicol.* **87** 1037–52
[6] He Q J and Huang Z L 2007 Template-directed growth and characterization of flowerlike porous carbonated hydroxyapatite spheres *Cryst. Res. Technol.* **42** 460–5
[7] Jones F 2001 Teeth and bones: applications of surface science to dental materials and related biomaterials *Surf. Sci. Rep.* **42** 75–205
[8] Catros S, Guillemot F, Lebraud E, Chanseau C, Perez S, Bareille R, Amédée J and Fricain J C 2010 Physico-chemical and biological properties of a nano-hydroxyapatite powder synthesized at room temperature *Irbm* **31** 226–33
[9] Huang Y, Song L, Huang T, Liu X, Xiao Y, Wu Y, Wu F and Gu Z 2010 Characterization and formation mechanism of nano-structured hydroxyapatite coatings deposited by the liquid precursor plasma spraying process *Biomed. Mater.* **5** 054113
[10] Ramya J R, Arul K T, Elayaraja K and Kalkura S N 2014 Physicochemical and biological properties of iron and zinc ions co-doped nanocrystalline hydroxyapatite, synthesized by ultrasonication *Ceram. Int.* **40** 16707–17
[11] Zhou H and Lee J 2011 Nanoscale hydroxyapatite particles for bone tissue engineering *Acta Biomater.* **7** 2769–81
[12] Sadat-Shojai M, Khorasani M-T, Dinpanah-Khoshdargi E and Jamshidi A 2013 Synthesis methods for nanosized hydroxyapatite with diverse structures *Acta Biomater.* **9** 7591–621
[13] Narayan R J, Kumta P N, Sfeir C, Lee D-H, Choi D and Olton D 2004 Nanostructured ceramics in medical devices: applications and prospects *Jom* **56** 38–43
[14] Chen F, Zhu Y-J, Zhang K-H, Wu J, Wang K-W, Tang Q-L and Mo X-M 2011 Europium-doped amorphous calcium phosphate porous nanospheres: preparation and application as luminescent drug carriers *Nanoscale Res. Lett.* **6** 67
[15] Ong H T, Loo J S C, Boey F Y C, Russell S J, Ma J and Peng K W 2008 Exploiting the high-affinity phosphonate-hydroxyapatite nanoparticle interaction for delivery of radiation and drugs *J. Nanoparticle Res.* **10** 141–50
[16] Cheng X and Kuhn L 2007 Chemotherapy drug delivery from calcium phosphate nanoparticles *Int. J. Nanomedicine* **2** 667–74
[17] Coelho C C, Sousa S R and Monteiro F J 2015 Heparinized nanohydroxyapatite/collagen granules for controlled release of vancomycin *J. Biomed. Mater. Res. Part A* **103** 3128–38
[18] Dasgupta S, Banerjee S S, Bandyopadhyay A and Bose S 2010 Zn- and Mg-doped hydroxyapatite nanoparticles for controlled release of protein *Langmuir* **26** 4958–64
[19] Shirkhanzadeh M and Azadegan M 1998 Formation of carbonate apatite on calcium phosphate coatings containing silver ions *J. Mater. Sci. Med.* **9** 385–91
[20] Kim T N, Feng Q L, Kim J O, Wu J, Wang H, Chen G C and Cui F Z 1998 Antimicrobial effects of metal ions (Ag^{+}, $Cu2^{+}$, $Zn2^{+}$) in hydroxyapatite *J. Mater. Sci., Mater. Med.* **9** 129–34
[21] Wu H-C, Wang T-W, Sun J-S, Wang W-H and Lin F-H 2007 A novel biomagnetic nanoparticle based on hydroxyapatite *Nanotechnology* **18** 165601
[22] Andronescu E, Ficai M, Voicu G, Ficai D, Maganu M and Ficai A 2010 Synthesis and characterization of collagen/hydroxyapatite: magnetite composite material for bone cancer treatment *J. Mater. Sci., Mater. Med.* **21** 2237–42
[23] Nayak A K 2010 Hydroxyapatite synthesis methodologies : an overview *Int. J. ChemTech Res.* **2** 903–7
[24] Oudadesse H, Mostafa A, Bui X, Gal Y, Le, Cathelineau G, Cnrs U M R, Rennes U D and Leclerc G 2011 Studies of doped biomimetic nano-hydroxyapatite/polymer matrix composites for applications in biomedical field *Recent Researches in Modern Medicine, Cambridge, United Kingdom* **4** 368–74
[25] Liu C, Huang Y, Shen W and Cui J 2001 Kinetics of hydroxyapatite precipitation at pH 10 to 11 *Biomaterials* **22** 301–6
[26] Uskoković V and Uskoković D P 2011 Nanosized hydroxyapatite and other calcium phosphates: chemistry of formation and application as drug and gene delivery agents *J. Biomed. Mater. Res. B. Appl. Biomater.* **96** 152–91
[27] Gómez-Morales J, Iafisco M, Delgado-López J M, Sarda S and Drouet C 2013 Progress on the preparation of nanocrystalline apatites and surface characterization: overview of fundamental and applied aspects *Prog. Cryst. Growth Charact. Mater.* **59** 1–46
[28] Castro F, Ferreira A, Rocha F, Vicente A and Teixeira J A 2013 Continuous-flow precipitation of hydroxyapatite at 37 °C in a meso oscillatory flow reactor *Ind. Eng. Chem. Res.* **52** 9816–21
[29] Reis N, Vicente A A, Teixeira J A and Mackley M R 2004 Residence times and mixing of a novel continuous oscillatory flow screening reactor *Chem. Eng. Sci.* **59** 4967–74
[30] Reis N, Harvey A, Mackley M R, Vicente A A and Teixeira J A 2005 Fluid mechanics and design aspects of a novel oscillatory flow screening mesoreactor *Chem. Eng. Res. Des.* **83** 357–71
[31] Reis N, Pereira R N, Vicente A A and Teixeira J A 2008 Enhanced gas−liquid mass transfer of an oscillatory constricted-tubular reactor *Ind. Eng. Chem. Res.* **47** 7190–201
[32] Jones A, Rigopoulos S and Zauner R 2005 Crystallization and precipitation engineering *Comput. Chem. Eng.* **29** 1159–66
[33] Lawton S, Steele G, Shering P, Engineering A, Park A, Sk C, Zhao L and Laird I 2009 Continuous crystallization of pharmaceuticals using a continuous oscillatory baffled crystallizer *Org. Process Res. Dev.* **13** 1357–63
[34] Dick W A and Tabatabai M A 1977 Determination of orthophosphate in aqueous-solutions containing labile organic and inorganic phosphorus-compounds *J. Env. Qual.* **6** 82–5
[35] Kokubo T and Takadama H 2006 How useful is SBF in predicting *in vivo* bone bioactivity? *Biomaterials* **27** 2907–15
[36] Bohner M and Lemaitre J 2009 Can bioactivity be tested *in vitro* with SBF solution? *Biomaterials* **30** 2175–9
[37] Kobayashi M, Kikutani T, Kokubo T and Nakamura T 1997 Direct bone formation on alumina bead composite *J. Biomed. Mater. Res.* **37** 554–65
[38] Kotani S, Fujita Y, Kitsugi T, Nakamura T, Yamamuro T and Ohtsuki C K T 1991 Bone bonding mechanism of beta-tricalcium phosphate *J. Biomed. Mater. Res.* **25** 1303–15
[39] Drouet C, Bosc F, Banu M, Largeot C, Combes C, Dechambre G, Estournès C, Raimbeaux G and Rey C 2009 Nanocrystalline apatites: from powders to biomaterials *Powder Technol.* **190** 118–22

[40] Koutsopoulos S 2002 Synthesis and characterization of hydroxyapatite crystals: a review study on the analytical methods *J. Biomed. Mater. Res.* **62** 600–12
[41] Depan D, Pesacreta T C and Misra R D K 2014 The synergistic effect of a hybrid graphene oxide–chitosan system and biomimetic mineralization on osteoblast functions *Biomaterials Science* **2** 264–74
[42] Chen L, Mccrate J M, Lee J C-M and Li H 2011 The role of surface charge on the uptake and biocompatibility of hydroxyapatite nanoparticles with osteoblast cells *Nanotechnology* **22** 105708
[43] Zhu P, Masuda Y and Koumoto K 2004 The effect of surface charge on hydroxyapatite nucleation *Biomaterials* **25** 3915–21
[44] Kim H M, Himeno T, Kokubo T and Nakamura T 2005 Process and kinetics of bonelike apatite formation on sintered hydroxyapatite in a simulated body fluid *Biomaterials* **26** 4366–73
[45] Bell L C, Posner A M and Quirk J P 1972 Surface charge characteristics of hydroxyapatite and fluorapatite *Nature* **239** 515–7
[46] Palazzo B, Iafisco M, Laforgia M, Margiotta N, Natile G, Bianchi C L, Walsh D, Mann S and Roveri N 2007 Biomimetic hydroxyapatite-drug nanocrystals as potential bone substitutes with antitumor drug delivery properties *Adv. Funct. Mater.* **17** 2180–8
[47] Ivanova T I, Frank-Kamenetskaya O V, Kol'tsov A B and Ugolkov V L 2001 Crystal structure of calcium-deficient carbonated hydroxyapatite. Thermal decomposition *J. Solid State Chem.* **160** 340–9
[48] Guo Y P, Yao Y B, Guo Y J and Ning C Q 2012 Hydrothermal fabrication of mesoporous carbonated hydroxyapatite microspheres for a drug delivery system *Microporous Mesoporous Mater.* **155** 245–51
[49] Rey C, Combes C, Drouet C, Sfihi H and Barroug A 2007 Physico-chemical properties of nanocrystalline apatites: implications for biominerals and biomaterials *Mater. Sci. Eng.* C **27** 198–205
[50] Luque de Castro M D and Priego-Capote F 2007 Ultrasound-assisted crystallization (sonocrystallization) *Ultrason. Sonochem.* **14** 717–24
[51] Aimable A, Jongen N, Testino A, Donnet M, Lemaître J, Hofmann H and Bowen P 2011 Precipitation of nanosized and nanostructured powders: process intensification and scale-out using a segmented flow tubular reactor (SFTR) *Chem. Eng. Technol.* **34** 344–52
[52] Rodan S B, Imai Y, Thiede M A, Wesolowski G, Thompson D, Bar-Shavit Z, Shull S, Mann K and Rodan G A 1987 Characterization of a human osteosarcoma cell line (Saos-2) with osteoblastic properties *Cancer Res.* **47** 4961–6
[53] Shi Z, Huang X, Cai Y, Tang R and Yang D 2009 Size effect of hydroxyapatite nanoparticles on proliferation and apoptosis of osteoblast-like cells *Acta Biomater.* **5** 338–45
[54] Bernhardt A, Thieme S, Domaschke H, Springer A, Rösen-Wolff A and Gelinsky M 2010 Crosstalk of osteoblast and osteoclast precursors on mineralized collagen-towards an *in vitro* model for bone remodeling *J. Biomed. Mater. Res.—Part* A **95** 848–56
[55] Balasundaram G, Sato M and Webster T J 2006 Using hydroxyapatite nanoparticles and decreased crystallinity to promote osteoblast adhesion similar to functionalizing with RGD *Biomaterials* **27** 2798–805
[56] Chou L, Marek B and Wagner W R 1999 Effects of hydroxylapatite coating crystallinity on biosolubility, cell attachment efficiency and proliferation *in vitro Biomaterials* **20** 977–85